Fracture Modeling of Rectangular Hollow Section Steel Braces

XIANG DING, DOUGLAS FOUTCH and SANG-WHAN HAN

Steel-braced frames are widely used in all regions of the United States including those with high levels of seismicity. Rectangular hollow sections (RHSs) are popular because of good section properties and ease of construction. A refined beam model has been developed which is efficient for use in finite element models of buildings. It accounts for local buckling and fracture in the brace and is shown to have good accuracy for nonlinear seismic analyses.

Braced frames possess sufficient lateral stiffness to inhibit large deformation under small to moderate earthquake motions. When the number of bays in one direction of a structure is limited, moment frames may not provide enough stiffness or be designed economically. Concentrically braced frames (CBFs) are more economical than eccentrically braced frames (EBFs), though the latter are highly recommended for earthquake resistance due to their good ductility (AISC, 2005b). Typical CBFs may use X-bracing, diagonal bracing, K-bracing, V-bracing, and inverted V-bracing. Architects prefer inverted V-bracing or diagonal bracing to X-bracing as the former provides for the convenience of door openings within the braced bays. The connections of the braces to gusset plates are much easier to fabricate than moment connections in moment frames so they are more economical to use.

Nonlinear behavior of braces and braced frames has been investigated by scientists since the 1970s. Numerous experimental studies have been performed on the inelastic cyclic response of bracing members for steel concentrically braced frames (Kahn and Hanson, 1976; Jain, Goel and Hanson, 1978; Popov and Black, 1981; Goel and El-Tayem, 1986). These investigations showed that bracing members typically exhibit nonsymmetrical hysteresis behavior, with strength degradation in compression and deformation accumulation of permanent elongation in tension. There are several principal factors affecting the behavior of braces.

Xiang Ding is principal structural engineer, Plant Engineering Services (Fluor), Baton Rouge, LA.

Douglas Foutch is professor of civil and environmental engineering, University of Illinois, Urbana, IL.

Sang-Whan Han is professor of architectural engineering, Hanyang University, Seoul, South Korea.

Slenderness Ratio, *KL/r*

K is the effective length factor, L is the unbraced length, and r is the radius of gyration. The energy dissipation capacity generally increases when the brace slenderness ratio is reduced (Remennikov and Walpole, 1997). The maximum brace slenderness ratio is specified in the code in order to provide a minimum level of energy dissipation. Tests performed on various brace specimens with different end conditions indicated that the effective length concept developed from the elastic theory is also applicable in the inelastic range to assess the ability of braces to dissipate seismic input energy.

Width-Thickness Ratio, *b/t*

Local buckling of the web or flanges of brace members due to large width-thickness ratios sometimes occurs before overall buckling and triggers overall buckling. Severe local buckling causes significant reductions in compressive capacity of the brace and leads to fracture in tension, which not only deprives the system of energy dissipation but also may result in collapse of the building. Local buckling issues are more difficult to simulate than overall buckling. For rectangular hollow sections (RHSs), the width of flanges or webs is the clear distance between webs or flanges less the inside corner radius on each side. If the corner radius is not known, the width shall be taken as the corresponding outside dimension minus three times the thickness. The thickness, t, shall be taken as the design wall thickness, per Section B3.12 of the AISC *Specification for Structural Steel Buildings* (AISC, 2005a).

Connection Restraint and Brace Configuration

Connection restraint at brace ends not only affects brace stiffness and strength but also affects fracture. Restraints at the ends of bracing members reduce their effective unbraced length, participate in energy-dissipation and, thereby, improve their seismic behavior. Brace slenderness can also be reduced by adopting an X-bracing configuration.

Ikeda and Mahin (1986) presented a model by assuming a deflected shape function for the brace and solving each of the axial displacement components. The analytic and experimental hysteresis loops were compared and found to be acceptable. Lee and Goel (1987) developed hysteresis models of a brace after studying the merits and demerits of Ikeda's model, Jain's model (Jain et al., 1978) and Liu and Goel's model (Liu, 1987). The analysis results were reported in good agreement with the corresponding experimental results.

Essentially, a brace carries axial force and bending moment. Remennikov and Walpole (1997) proposed a P-M interaction yield surface function based on stepwise regression analysis. Assuming the plastic hinge occurs at the brace midspan, the right half was taken out to decompose its axial deformation into elastic axial deformation, geometric shortening deformation, plastic hinge deformation, and tensile yield deformation. It was suggested that more stringent regulations should be imposed on the use of V or inverted V-braced frames in high seismicity areas. There are some requirements for those braced frames (AISC, 2005b): beams intersected by the V or inverted V-braces should not fail under the axial force of one brace when the other brace has buckled; those beams should also be laterally braced to prevent lateral buckling.

EXPERIMENTAL STUDIES ON RHS BRACES

Rectangular hollow sections are very effective in compression and their use for braces forms an efficient means of resisting lateral seismic loads and satisfying code limits on maximum brace slenderness ratio. Moreover, RHSs have large flexural and torsional stiffness due to their hollow and closed shape. Studies by Gugerli and Goel (1984) and Lee and Goel (1987) showed that bracing members made of RHSs experienced premature fractures soon after severe local buckling even though those sections satisfied the AISC requirements for compact sections. Lee and Goel (1987) reported the experiments on seismic behavior of hollow and concrete-filled square tubular bracing members. The test results showed that when the width-thickness ratio of hollow specimens was reduced from 30 to 14, the initial and the severe local buckling were much delayed and consequently, the fracture life increased. In the test, another veiled fact is that semi-fixed braces can dissipate more energy than fixed braces. Although the loading history emphasized compression, the test results of some specimens can be utilized for regression analysis of fracture life in this study.

Recently, an experimental study on buckling and fracture of single RHS steel brace specimens with nominal yielding strength of 345 MPa (50 ksi) has been conducted in Korea (Han, Wook and Foutch, 2006). The slenderness ratio, KL/r, ranges from 70 to 90 for the specimens. A typical test scheme and the load history are shown in Figures 1 and 2, respectively (1 mm = 0.0394 in.). Although the story displacement is set up to reach 5% drift, the ultimate story drifts before brace fracture were between 2% and 4%.

The experimental results showed that the occurrence and severity of the local buckling, and the fracture mode and life, depend strongly on *b/t* ratios of the specimens. Based on the observation of local and overall buckling in the test, the sequence of buckling was classified into three buckling modes: local buckling mode, overall-local buckling mode, and overall buckling mode (Han et al., 2006).

Local Buckling Mode (L Mode)

The specimens in the L mode experienced local buckling prior to overall buckling when the compression force reached a buckling load, P_{cr}. In a few cycles after local buckling occurred, the specimens fractured at the midspan section under

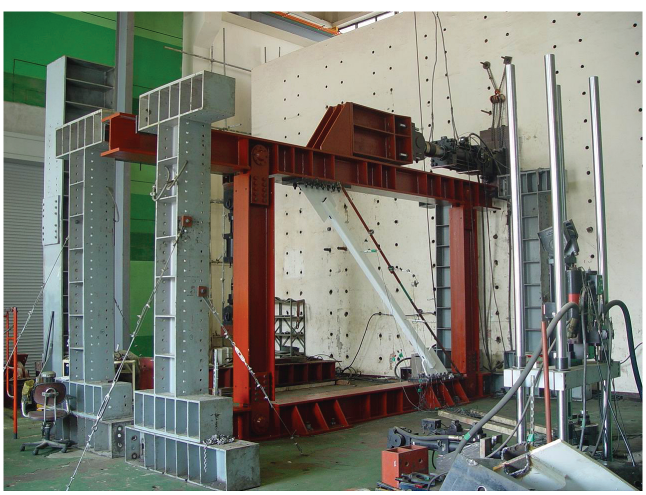

Fig. 1. A typical test specimen and the loading scheme.

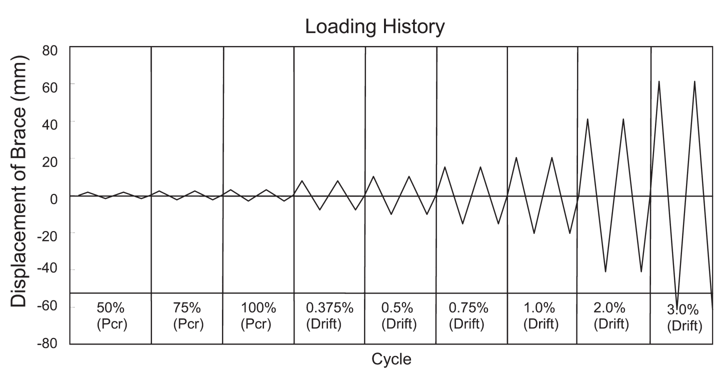

Fig. 2. Loading history of the test braces.

tension due to large plastic deformation caused by severe local buckling. Specimens with a noncompact width-thickness ratio (>18) failed in this sequence (L mode).

Overall-Local Buckling Mode (O-L Mode)

In this mode, bracing members experienced overall buckling (Figure 3) and the compression force reached a buckling load, P_{cr}, prior to the occurrence of local buckling. On the seventh cycle of compression, with a drift ratio of 0.375%, overall buckling occurred. On cycles 13 to 16, compression local buckling occurred. With an increase in the loading cycle, local buckling became more severe (Figure 4). In the following two cycles, fine wrinkles appeared where local buckling was present. Cracks were observed at the two corners near the flange opposite to the overall buckling direction ("inner flange") at the midspan. On the following cycles of tension, the cracks were propagated across the section and led to fracture at the midspan (see Figure 3d).

In this study, specimens with moderate *b/t* ratios of 13 to 18 fractured in this mode. The brace hysteresis curve under cyclic load is shown in Figure 5. Compared with specimens in the L mode, O-L mode specimens had better hysteresis behavior. This is attributed to a smaller *b/t* ratio that delayed the occurrence of local buckling and reduced the severity of local buckling in a given loading cycle.

(a) Overall buckling (–0.375%).

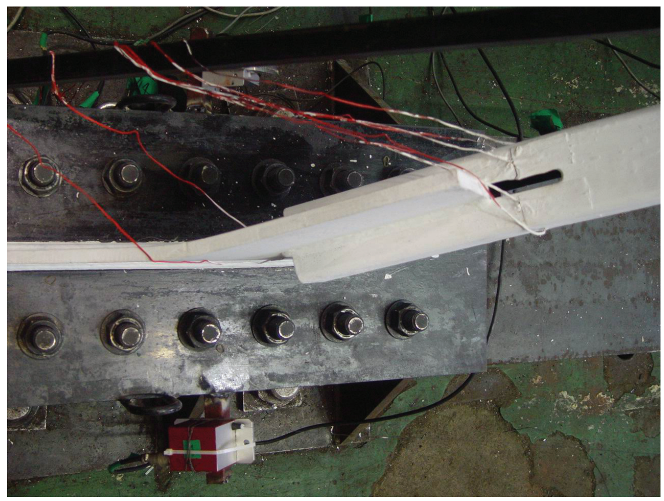

(b) Gusset plate buckling (–2%).

(c) Local buckling (–2%).

(d) Detail of fracture.

Fig. 3. Setup, buckling and fracture of specimen 100×100×6 #1 (O-L mode).

Overall Buckling Mode (O Mode)

Specimens with *b/t* ratios less than 13 fell into this category. Early in the loading stage, these specimens fractured under tension at the slotted end of the specimen, with appreciable distortion at the fracture section. No local buckling occurred, but overall buckling in these specimens was observed. It is important to note that the details of slots and connections between bracing member and gusset plates in the specimens followed the AISC *Steel Construction Manual* (AISC, 2005c). If the net section at the slot had the strength required by the AISC *Seismic Provisions* (AISC, 2005b), the overall buckling may successfully bring secondary bending moment to the gusset plate, and potentially a plastic hinge could be developed there.

Fracture can always be attributed to cracks in the wall of the brace due to severe plasticity caused by local buckling or excessive elongation. The local buckling mode and the overall-local buckling mode accompany relatively ductile failure in which fracture occurs at midspan due to large cyclic plastic deformation. The overall buckling mode will lead to brittle and unfavorable failure in which fracture occurs due to high concentrated stress at the sections with least net area or with initial fabrication defects such as a sharp cut at slots and embedded-cracks in or adjacent to welds, etc. However, reinforcement at weak net sections at slots and good fabrication practices can prevent braces from fracturing there. Therefore, brace fracture in the local buckling mode and the overall-local buckling mode will be discussed later.

When a single brace is subjected to displacement-controlled cyclic loads, the main failure mode is fracture in tension cycles. Local buckling eventually develops in the plastic hinge that forms in the brace. Fracture can be always attributed to the cracks that develop in the wall of the brace due to severe plasticity caused by local buckling. Fracture of the brace then rapidly occurs when it is subsequently pulled in tension. The tensile stiffness of the braces will decrease under cyclic loads because overall buckling results in the secondary bending moment and local buckling reduces the effective cross-section area at the midspan, which lead to premature tensile yielding. The brace slackness due to the tensile elongation brings a "free play" before the brace recovers the compressive stiffness in the subsequent compression cycles (Figure 5). Therefore, the post-buckling stiffness of those bracing systems declines very rapidly.

FINITE ELEMENT MODELING OF BRACES AND BRACE CONNECTIONS

Modeling of Brace Connections

Bracing connections act quite differently from the postulated ideal pin-joints. Gusset plates provide braces with stronger in-plane restraint than out-of-plane restraint, so V- or inverted-V-braces made of square hollow tubes are more likely to buckle out of plane due to longer effective unbraced length out of plane. This is also true for X braces due to the intersecting joint. There should be enough space left between these braces and partitions or cladding within the bay of braced frames to allow this deformation to occur without impacting walls or claddings. Out-of-plane plastic deformation capacity at a gusset plate is recommended for design of the joints (AISC, 2005b), as shown in Figure 6.

In the brace tests in Korea (Han et al., 2006), the plastic zone in the gusset plates caused by out-of-plane bending moment, as shown in Figure 7, is about 3*t* wide and 1*t* away

Fig. 4. Local buckling of brace 100×100×6.

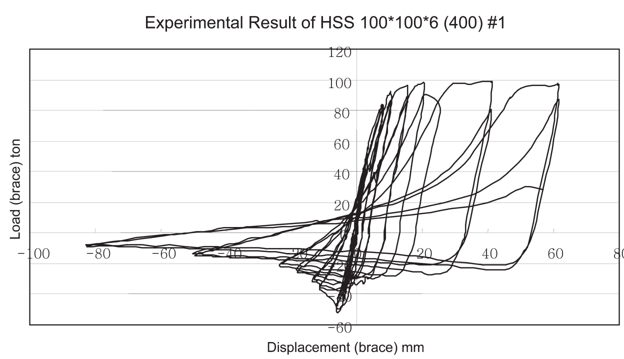

Fig. 5. Experimental hysteresis loops of specimen #1.

from the brace end, where t is thickness of the gusset plate. The gusset plates remain almost elastic elsewhere. Thus, gusset plates can be modeled as two beam segments (B33 in Abaqus). Considering the restraint from welds, twice the thickness of the gusset plate is used as the breadth of the beam element for the rest of the gusset plate other than the segment for plastic hinge. The modeling scheme of the brace connections is as shown in Figure 6. Each brace is modeled by 20 beam elements, and brace fracture is modeled by a special Abaqus user element discussed later.

Refined Beam Element Model

A refined beam element model has been widely used to simulate bracing members and struts. By dividing a brace into many segments, geometrical nonlinearity of the brace is easily included. The effect of overall buckling as well as slenderness ratio can be taken into account by the refined beam element model in the Abaqus program. A single beam cannot adequately detect the plasticity along the whole length. More accurate material and geometrical nonlinearity is reflected in the refined beam modeling.

A numerical simulation for specimen #1 of the brace tests in Korea (Han et al. 2006) has been selected to examine the refined modeling for Abaqus. The single brace with a length 3250 mm (10 ft 4 in.) is divided into about 20 elements to ensure good accuracy of geometrical nonlinearity. The gusset plates are 16 mm (⅝ in.) thick. The out-of-plane imperfection ratio of the strut is assumed as 0.1% (Gu and Chan, 2004). The out-of-plane imperfection curvature is assumed parabolic. Steel strain hardening ratio is set as 1%. Figures 5 and 8 are, respectively, the experimental and computed hysteresis loops of Specimen HSS100×100×6 #1 (HSS4×4×¼ in US units, 1 ton = 2.205 kips). Local buckling of the brace flange before fracture does not affect the hysteresis loop of the brace to a large degree. Accordingly, the refined beam element model can be applied to nonlinear analysis of braces.

Partial Shell Element Model

To study fracture of braces of a structural system at grain size level is not feasible for building structures. Fracture of structural metals under tensile loading usually occurs by a damage accumulation process involving void nucleation, void growth, and void coalescence (Venson and Voyiadjis, 2001). Material failure is controlled primarily by void growth and void coalescence, so most fatigue and fracture studies of metal are done in the field of continuum mechanics. Unless fine element types such as shell elements or solid elements are used for brace analyses, we cannot determine the actual concentrative and excessive strain and stress at the fracture location of the brace. One hinge region needs about 3,000 shell elements to simulate the phenomena (Figure 9). Due to very large computational work involved, shell element model simulation for crack development is not realistic for nonlinear dynamic analyses of building structural systems.

However, shell element modeling can be used to investigate local buckling of braces because beam element analysis cannot address that solely. In order to save computational time, the shell mesh only applies to the region near the local buckling and beam elements are used elsewhere. A rigid pad connects the beam element and shell elements at each transition, which was proven not to induce stress concentration (Figures 12 and 13). This model is called a partial shell element model, as shown in Figure 10. The computed hysteresis loops of the test braces in Korea using a partial shell

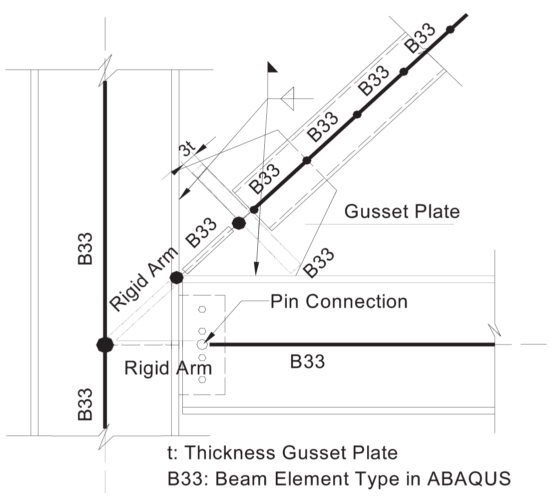

Fig. 6. Modeling scheme of the connection.

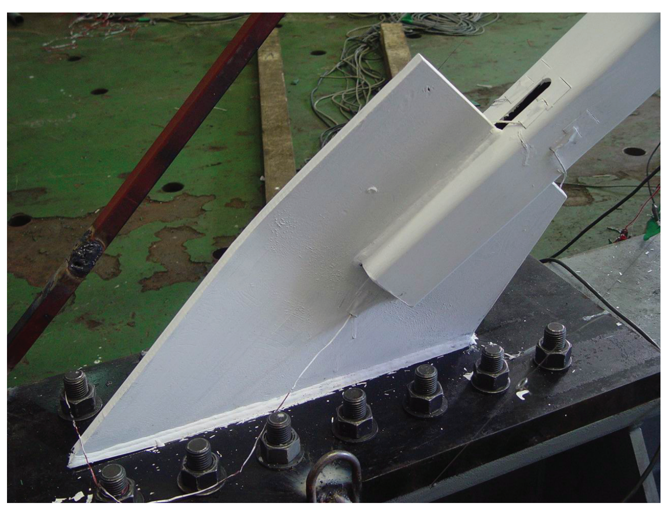

Fig. 7. Plastic zone of gusset plate.

element model and a full shell element model are identical. The buckling load and load time of the test braces computed by this model match the test results very well. Figures 4 and 11 show the local buckling deformation of the test specimen HSS100×100×6 and the simulation of the partial shell model. Figures 12 and 13 display the high stress of more than 0.1 ton/mm^2 (142 ksi) due to excessive plastic deformation where local buckling occurs. The partial shell element model also predicts the local buckling load of RHS braces under monotonic compression load very accurately (Figures 4, 11 and 14).

Although local buckling dominates the fracture as discussed later, by comparing the hysteresis curves of a brace specimen by the refined beam element model and the partial shell element model (Figure 15), it is obvious that local buckling does not affect the overall stiffness of braces to a large degree. The results of the two modelings match the experimental one very well (Figures 5, 8 and 15). For braced frames, the refined beam element model is good for brace simulations if local buckling and fracture can be detected in the model.

Local Buckling and Fracture Modeling

Inelastic local buckling in braces also accompanies plastic hinge development. In order to detect the concentrated deformation at local buckling, we can put appropriately finer beam elements at the places where the hinge could occur, most likely the midspan. By comparing the strains of these beam elements and those of the corresponding shell elements and the test results, we can find a way to determine local buckling and fracture just by using beam elements. From the

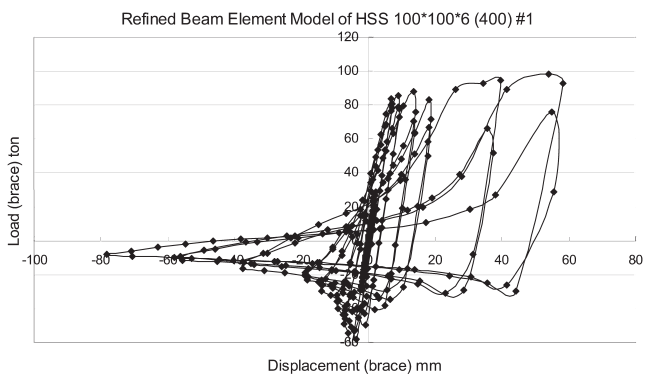

Fig. 8. Computed hysteresis loops of specimen #1.

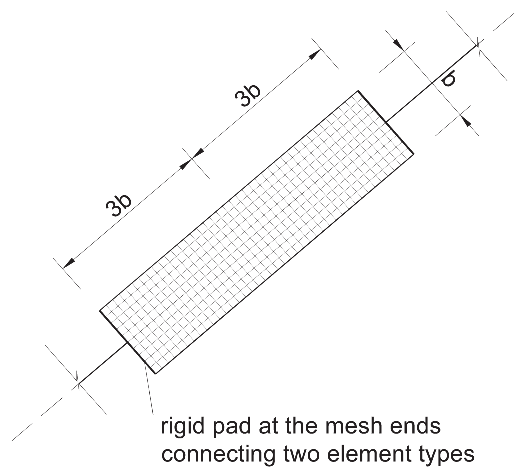

Fig. 9. Shell mesh for detecting local buckling.

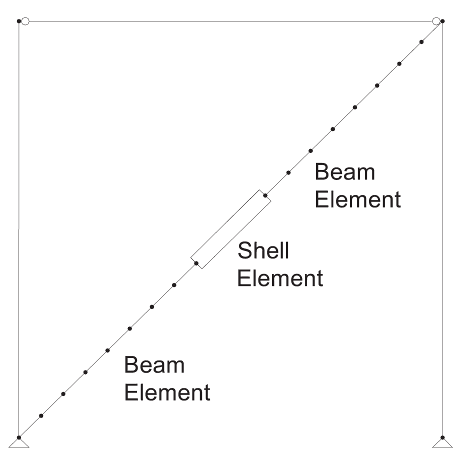

Fig. 10. Finite element scheme for the test.

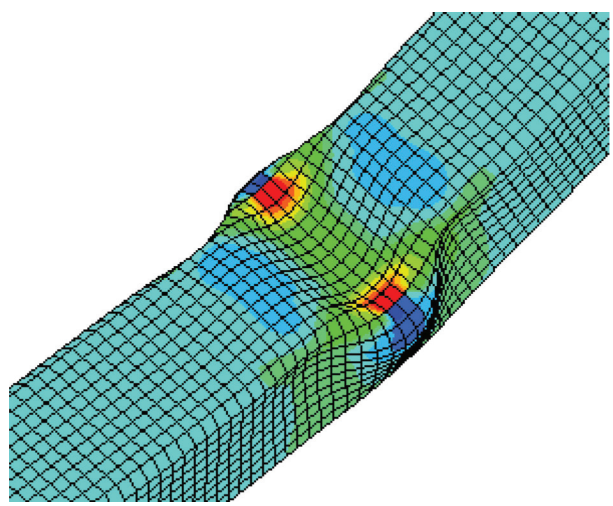

Fig. 11. Shell mesh simulation of brace 100×100×6.

photos of the test specimens and the finite element analysis results (Figures 4, 12 and 14), we can see that half of the cross-section size is a very good value as the length of those finer beam elements. Actually, the local buckling range of an RHS brace along its length is about equal to the flange width.

Therefore, a beam-connector-beam (BCB) element model is proposed. The two beam elements are used to predict local buckling and fracture while the connector element is used as a switch to simulate the discontinuity of beam after fracture because the beam elements cannot be disconnected by themselves. As shown in Figure 16, and as defined in the user element BCB element subroutine for Abaqus (2004), node I and node J are the nodes of element 1; node K and node L are the nodes of element 2. Between the two elements, a connector element with six degrees of freedom is set to connect node J and node K. The stiffness matrix of this connector element can be composed of the stiffness of the six springs in the three translational directions and the three rotational directions, which are extremely large before fracture and extremely small after fracture. The real-time nodal displacements can be monitored in Abaqus so as to determine the status of the two beam elements. Both of them are modeled as fiber beam elements in the Abaqus subroutine. Eight fibers (using brace material) for each beam element are employed to carry out the real-time detection of nominal stress and strain. One fiber is placed at each corner of the brace and one at the centerline of each face. Therefore, nominal stress and strain at the four corners and the four face centers of the assumed fracture section can be obtained at each load step to judge local buckling and fracture of the brace.

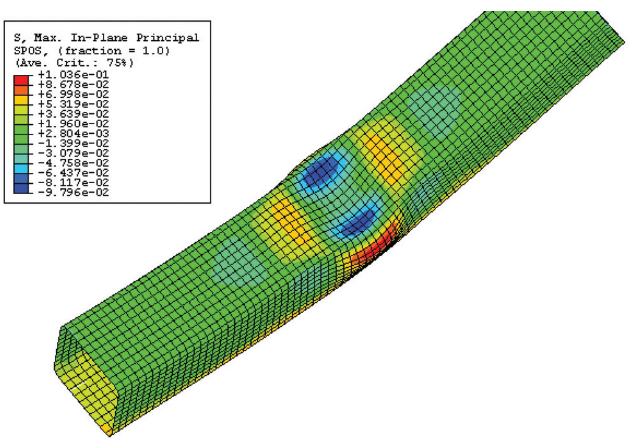

Fig. 12. Outside stress of brace 100×100×6.

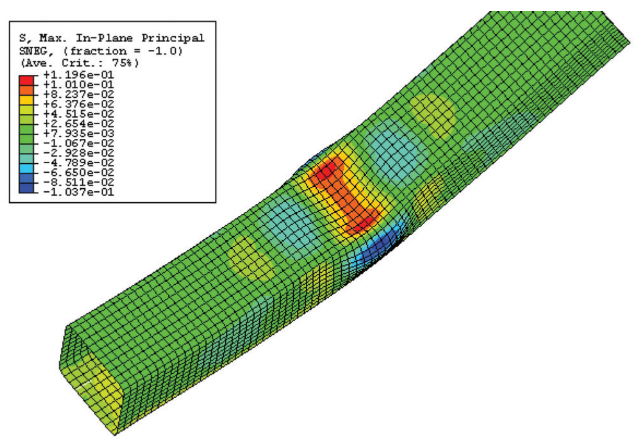

Fig. 13. Inside stress of brace 100×100×6.

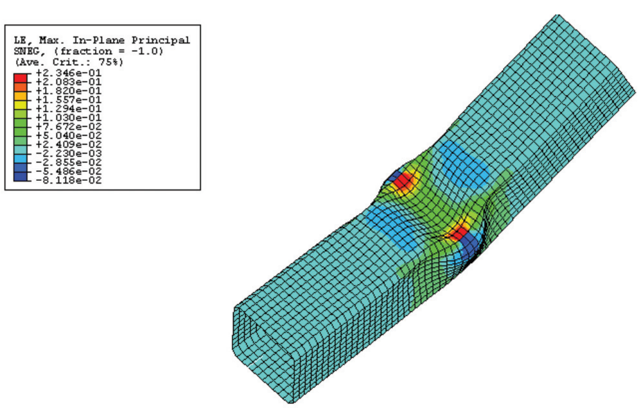

Fig. 14. The deformation upon local buckling.

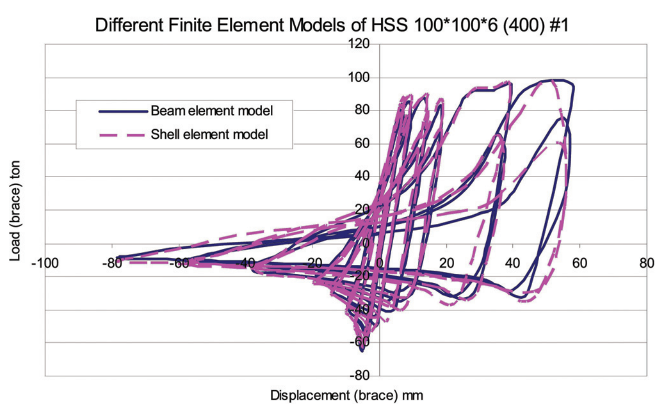

Fig. 15. Hysteresis curves of refined beam element model and partial shell element model.

Table 1. Test and Computed Results of Local Buckling and Fracture of Tube Braces Under Cyclic Loads						
Test No.	RHS Specimen, mm	Local Buckling Time, s	Fracture Time, s	Fracture Strain	Boundaries and Reversal Loads	Reference
1	100×100×6	29.9 [29.7]	36.7 [36.2]	0.32	Semi-fixed, load 3	Han et al. (2006)
2	125×125×6	26.0 [25.7]	32.7 [32.7]	0.32	Semi-fixed, load 3	Han et al. (2006)
3	125×125×4.76	1.46 [1.68]	9.0 [8.99]	0.22	Semi-fixed, load 1	Lee et al. (1987)
4	125×125×4.76	1.56 [1.68]	10.8 [10.4]	0.22	Fixed, load 1	Lee et al. (1987)
5	100×100×6.35	13.8 [15.9]	21.0 [20.9]	0.14	Fixed, load 1	Lee et al. (1987)
6	100×100×6.35	10.0 [12.0]	16.7 [16.3]	0.14	Fixed, load 2	Lee et al. (1987)

LOCAL BUCKLING AND FRACTURE CRITERIA FOR BRACES

Nominal Strain of Local Buckling

Although fracture spreads across the entire section at complete failure, it starts at the flange opposite to the overall buckling direction (the "inner flange"), as shown in Figure 17. For convenience, the other flange of the RHS brace is called the "outer flange." Figures 17 and 18, respectively, illustrate the nominal strains at the inner side and outer side of the midspan cross section of a brace 100×100×6 of the test in Korea (test no. 1 in Table 1), which were calculated by the BCB element.

As plastic hinging due to bending moment was obviously experienced at the midspan of the brace, the second-order bending moment played a very important role due to *P-M* interaction and *P*-Δ effect. For the outer flange at the midspan, the compressive axial strain is overshadowed by the tensile strain caused by the bending moment when the brace is in compression. For the inner flange at the midspan, the compressive strain is deteriorated by the compressive axial strain caused by the bending moment. Consequently, the nominal deformation at the inner flange was more severe than that at the outer flange, as observed in the Korean test. Therefore, local buckling always starts with the inner flange.

Nominal strain of local buckling, ε_B, is defined as the strain of the inner flange fiber calculated by the BCB element through using the refined beam element model when local buckling occurs there. Local buckling can be detected in physical tests or numerical simulation using the partial shell element model, as shown in Figure 14. The greater the width-thickness ratio, the smaller the nominal strain of local

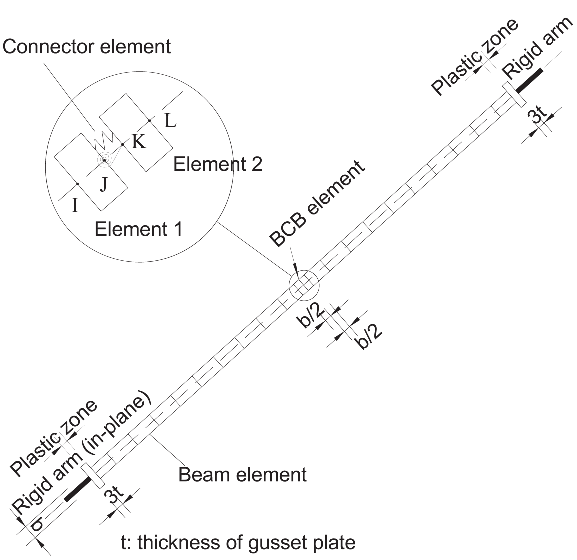

Fig. 16. Element dividing in refined beam element model of a brace.

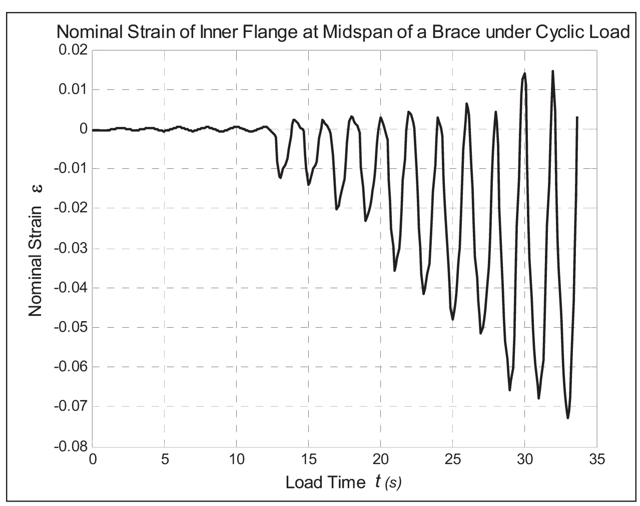

Fig. 17. Nominal strain of brace inner flange.

buckling would be (Figure 19). The local buckling criterion for a tube section can be obtained by regression analysis of the eight experimental results:

$$\varepsilon_B = 0.909/\lambda^{0.147} - 0.542 \tag{1}$$

where $\lambda = b/t$ and $5 \le \lambda \le 30$. The influence of overall buckling, which mainly depends on the slenderness ratio, KL/r, can be interpreted through the nominal strain at the midspan. Figure 20 shows that the slenderness ratio, KL/r, does not affect nominal strain criterion of local buckling at the midspan. Although the slenderness ratio affects P-M interaction at the midspan, which is already reflected in the (compressive) strain of the inner flange fiber at the midspan, how the strain/stress comes from the far ends to there does not influence the nominal strain criterion of local buckling according to Saint Venant's Principle.

In this way, local buckling of a brace can be easily discerned without using a fine mesh of shell elements.

Strain-Based Fracture Criterion

Local buckling usually contributes to large concentrated deformation leading to fracture. Local buckling deformation causes the local bending moment at the inner flange and the webs, otherwise the stress and strain at the flanges and the webs should be nearly uniformly distributed along the thickness direction. In fact, upon local buckling, the excessive out-of-plane tube wall deformation and the corresponding stress are so dominant that the strain at the bulb increases very quickly and may reach 0.23 or greater (Figure 14) while local buckling becomes severe. Because the stiffness of the post-buckling inner flange is small, the axial stress has to be redistributed to the two nearby corners. Therefore, the fine transverse plastic wrinkles will form at the two corners, as shown in Figure 4. This is also the location where residual stress lies due to the forming process of the RHS section.

Mini cracks usually accompany the fine wrinkles. If the axial force changes to tension in the subsequent cyclic loading, the corners near the inner flange carry major tension even though the buckled inner flange beside the two corners may be pulled straight. As the axial force increases, those cracks develop and propagate. Finally, at the two corners, the cracks develop rapidly so that fracture inevitably occurs from the two corners to the whole cross section, as shown in Figure 3(d).

Low-cycle fatigue is a serious problem for braced structures subjected to earthquakes because seismic vibration of

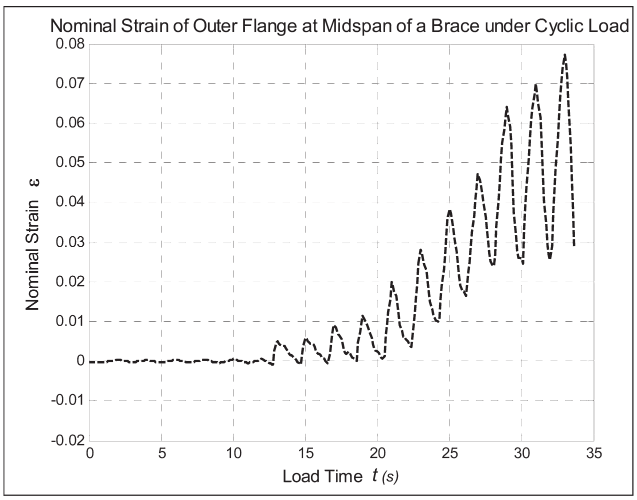

Fig. 18. Nominal strain of brace outer flange.

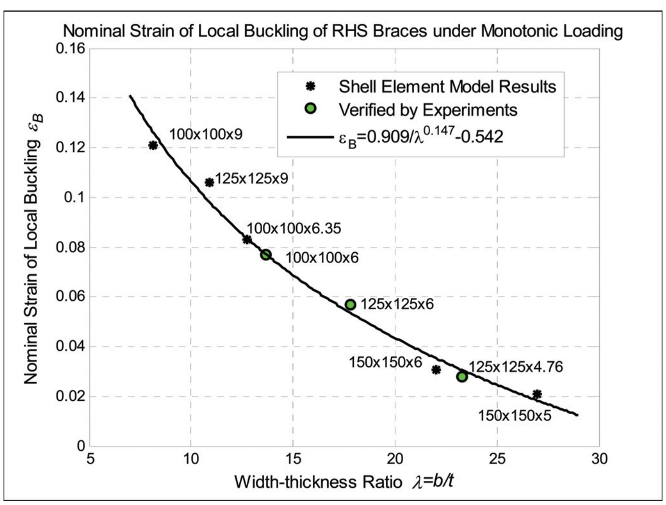

Fig. 19. Nominal strain of local buckling of tube braces with different width-thickness ratios.

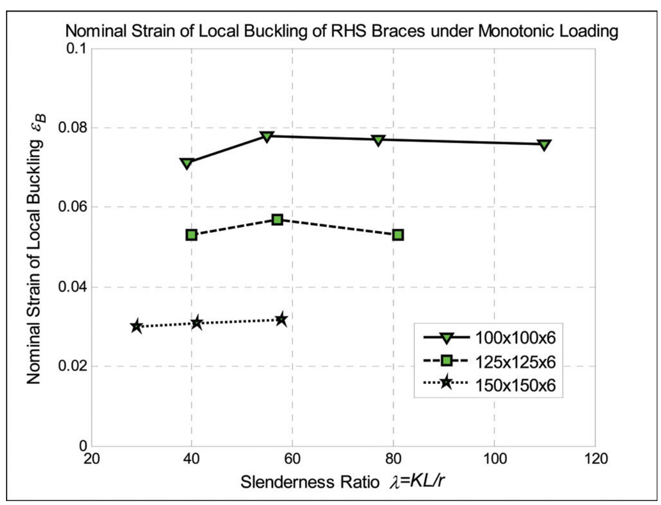

Fig. 20. Nominal strain of local buckling of tube braces with different slenderness ratios.

structures may cause considerable damage accumulation. How to determine damage accumulation of braces at the member level remains unclear. A strain-based damage criterion at the inner flanges of RHS braces is proposed later.

Major parameters influencing fracture life are brace slenderness ratio, section property, boundary condition, brace imperfections, material properties (such as Young's modulus, elongation rate, yielding strength, ultimate tensile strength), and width-thickness ratio. The first four factors and overall buckling have been reflected in the nominal strain of the inner flange. Material and geometrical information can be input in the modeling.

Fracture strain is a very important index of ductility. The true fracture strain, ε_f, is the true strain based on the original area, A_0, and the area after fracture, A_f (Ling, 1996), where

$$\varepsilon_f = \ln \frac{A_0}{A_f} \tag{2}$$

This parameter represents the maximum true strain that the material can withstand before fracture and is analogous to the ultimate uniaxial tensile strain ε_{cr} at the end of the engineering stress-strain curve. In structural engineering, ε_{cr} is equivalently taken as the fracture strain (Ling, 1996; Han et al., 2006). ε_{cr} can be determined by coupon tests of the ultimate strain at the necking location of a steel tensile specimen under monotonic uniaxial tensile loading. Generally, the fracture strain of structural steel varies from 0.05 for brittle steel to 0.70, or even greater, for ductile steel.

The damage/shear strain dependence for monotonic loading can be described by the power law (Lemaritre and Chaboche, 1975):

$$\omega = b\varepsilon^a \tag{3}$$

where ω is an index of damage accumulation; a, b are functions of stresses and temperature.

For undamaged material, $\omega = 0$. At fracture, when ε reaches ε_{cr}, $\omega = 1$, so $b = 1/\varepsilon_{cr}^a$. So for monotonic loading

$$\omega = \left(\frac{\varepsilon}{\varepsilon_{cr}}\right)^a \tag{4}$$

For non-monotonic loading

$$\omega = \sum_{i=1}^{N} \left(\frac{|\Delta\varepsilon_i|}{\varepsilon_{cr}}\right)^a \tag{5}$$

$$\Delta\varepsilon_i = \varepsilon_i - \varepsilon_{i-1} \tag{6}$$

where

ε_i = strain amplitude of cycle i

ε_{i-1} = strain amplitude of cycle $i-1$

Because local buckling brings large deformation and severe damage, local buckling should be detected first. We define $\Delta\varepsilon_{ic}$ as strain amplitude in compression cycles. Local buckling will happen for braces categorized in L mode or O-L mode if the local buckling index, BI, which evaluates initiation of local buckling, is equal to or greater than 1.0,

$$\mathrm{BI} = \frac{|\Delta\varepsilon_{ic}|}{\phi_B \varepsilon_B} \tag{7}$$

where

ϕ_B = local buckling resistance factor for ε_B in order to consider plastic deformation accumulation due to previous cycles of non-monotonic loading before local buckling

ϕ_B can be derived as

$$\phi_B = 1 - \eta \sum_{i}^{L} \left(\frac{|\Delta\varepsilon_{ic}|}{\varepsilon_B}\right)^{\gamma_B} \tag{8}$$

where

L = number of loading cycles until local buckling occurs

η = parameter for computing the local buckling resistance factor

γ_B = parameter for computing the local buckling resistance factor

η and γ_B can be determined by regression analysis of test results of local buckling. It would be expected that ϕ_B is close to 1 for braces with large b/t, where local buckling is close to elastic buckling. For small b/t ratios, yielding will occur before buckling and inelastic buckling occurs. For monotonic loading, $\phi_B = 1$. The local buckling criterion $\phi_B \varepsilon_B$ is decreasing when a brace is under cyclic loading. Hence, it needs to be updated at each cycle.

The damage index, DI, which evaluates fracture life, is composed of two parts: one accounts for deformation before local buckling; the other is for damage accumulation after local buckling.

$$\mathrm{DI} = \sum_{i=1}^{L-1} \left(\frac{|\Delta\varepsilon_i|}{\varepsilon_{cr}}\right)^{\alpha} + \sum_{i=L}^{N} \left(\frac{|\Delta\varepsilon_i|}{\varepsilon_{cr}}\right)^{\beta} \tag{9}$$

where

α = parameter for computing the damage index, which can be determined by regression analysis of experiment results

β = parameter for computing the damage index, which can be determined by regression analysis of experiment results

N = the number of loading cycles before fracture

For example, if the yield strength of a steel bar is 345 MPa (50 ksi), $|\Delta\sigma_i|$ = 220 MPa (31.9 ksi) [changes linearly between −110 MPa (−16 ksi) and 110 MPa (16 ksi)], $|\Delta\varepsilon_i| = |\Delta\sigma_i|/E = 0.0011$, $\varepsilon_{cr} = 0.28$, if $\alpha = 2$ and no local buckling occurs, then the fracture cycles $N = (\varepsilon_{cr}/|\Delta\varepsilon_i|)^{\alpha}/2 = (0.28/0.0011)^2/2 = 32{,}397$.

A brace cannot fracture while the section fibers are fully in compression (Han et al., 2006). When the damage index, DI, of any fiber in the two beam elements of the BCB elements reaches 1.0, and the nominal stress of that fiber reaches the tensile yield stress, fracture will occur for a brace categorized in L mode or O-L mode.

In the subsequent discussion, the parameters in the preceding equations will be determined, and the method verified.

Application and Verification of the Modeling

The refined beam element model with the BCB elements has been completed and tested as follows. For verification, six specimens from two separate tests are considered, as shown in Table 1. Test 1 and test 2 have been described in this chapter; Tests 3 through 6 were completed by Lee and Goel (1987). Tests 1 through 3 are used to obtain values of the parameters η and γ_B, α and β in Equations 8 and 9 by the regression analysis on the buckling times, and the fracture times, respectively. These values are determined as $\eta = 0.15$, $\gamma_B = 2.73$, $\alpha = 2.73$, and $\beta = 1.47$. The computed results of tests 4 through 6 are compared with the experimental results to justify these two parameters for regular building tube braces with *b/t* values from 15.7 to 26.3. The bracing length is 3250 mm (10 ft 8 in.).

For convenience, HSS5×5×3⁄16 and HSS4×4×1⁄4 in the Lee and Goel test are converted to 125×125×4.76 and 100×100×6.35, respectively. In Table 1 and Figures 21 through 26, load time does not mean the actual loading time. It represents one loading cycle per “2 seconds” in the load history description. In the table, the numbers in the brackets are the computed local buckling time or the computed fracture time.

Reversal load 3 is shown in Figure 2. Reversal load 1 and reversal load 2 were defined in the report by Lee and Goel (1987). The cyclic load histories are also shown in Figures 21 through 26. Figures 21a through 26a show when local buckling initiates, when fracture occurs, and how the damage index increases. Figures 21b through 26b show how the local buckling strain resistance factor decreases after a few cycles of the loads and the local buckling index approaches 1.0. Figures 21c through 26c show the nominal strain and the nominal stress (1 MPa = 0.145 ksi) at the inner flange in the two beam elements of BCB beside the cross section at the midspan. The difference between a fixed boundary condition and a semi-fixed one is that the fixed ones have the gusset plates stiffened to prevent hinging in the gusset plate and the semi-fixed ones do not.

Figures 21a, b and c show the results for a member with a low *b/t* ratio (13.6) and large fracture strain (0.32). Several large cycles of axial displacement are applied before local buckling occurs, and several more before fracture occurs. The axial deflection reaches 50 mm (1.97 in.) before fracture occurs. Note that ϕ_B becomes smaller with load cycles for this member with a small *b/t*. Figures 22a, b, and c show the results for a member with *b/t* = 17.8. For this case, the axial deflection reaches about 40 mm (1.57 in.), and the time to failure decreases because of the larger *b/t*. However, both of these specimens show excellent ductile behavior. Figure 23 series show the results for a member with *b/t* = 23.3 and fracture strain 0.22. For this case, local buckling occurs while $\phi_B \cong 10$. The ductility of the specimens in Tests 3 and 4 is not so good because of the larger *b/t* and lower fracture strain. Note that ϕ_B =1 until local buckling occurs in this member with large *b/t*. The same member size and loading pattern were used for the member response shown in Figure 24. The only difference is that the gusset plate is stiffened out of plane for the member shown in Figure 24 but not the one in Figure 23. The member in Figure 24 performed only slightly better than the one in Figure 23. In Figure 25a, the tested local buckling time occurs prior to the calculated local buckling time. The reason could be some large section imperfection or some deviation of material property. The Figures 25 and 26 series show the results for a member with *b/t* = 12.7 and fracture strain 0.14. Because of the low *b/t* value, several large cycles are required for local buckling to occur. The ductility, although reasonably good, is reduced because of the low value of fracture strain.

Figures 21a through 26a show that the portion of DI before local buckling is only about 5% to 20%. After local buckling, DI increases rapidly. It reveals that local buckling is the cause of brace fracture at the midspan.

The prediction of local buckling and fracture of braces is more than acceptable for analysis of building structures. Fracture predictions of the six brace specimens are very accurate and slightly conservative. Therefore, brace fracture modeling for steel braced frames is not only feasible but also applicable.

It should be noted that these computed results are consistently good even though the test loading sequence were different for the two testing programs. The tests by Han et al. (2006) used a symmetrical loading sequence with equal displacements in compression and tension, while the Lee and Goel (1987) tests used loadings where compressive displacements increased but the maximum tension ones were a small constant for each cycle. So, load 3 (Table 1) is potentially more damaging because of the large strain excursions applied in tension. Also, the specimens considered covered large ranges of width-thickness ratio and fracture strain.

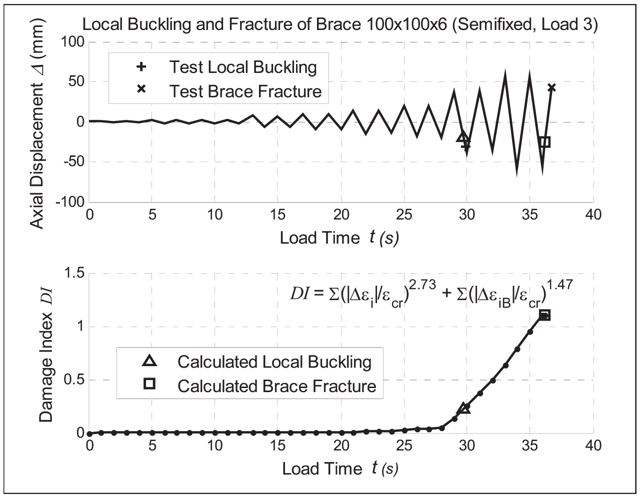

Fig. 21a. Local buckling and fracture of brace 100×100×6 semi-fixed under load 3.

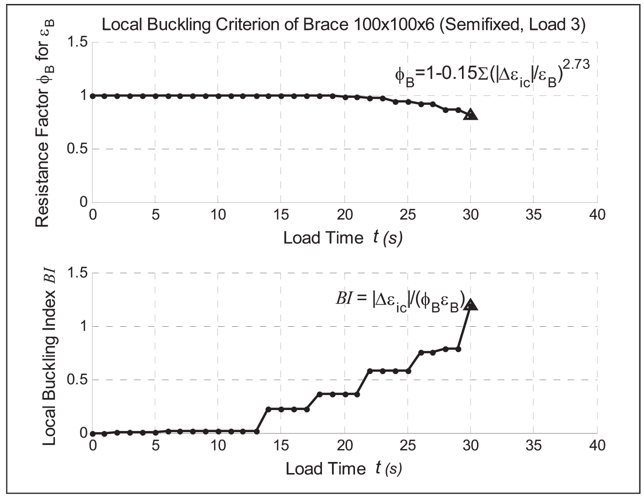

Fig. 21b. Local buckling index of brace 100×100×6 semi-fixed under load 3.

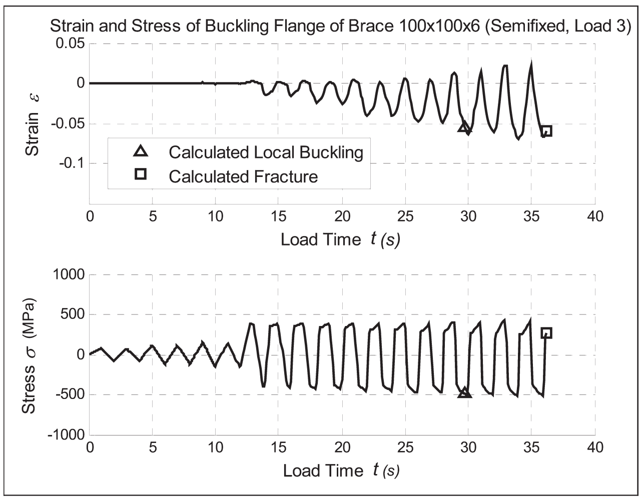

Fig. 21c. Nominal strain and stress of brace 100×100×6 semi-fixed under load 3.

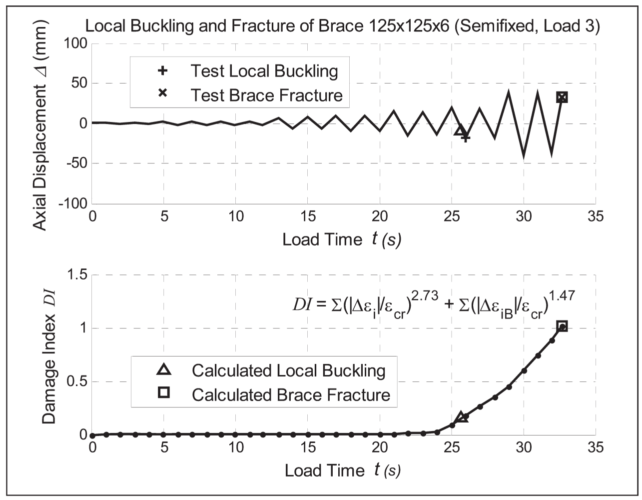

Fig. 22a. Local buckling and fracture of brace 125×125×6 semi-fixed under load 3.

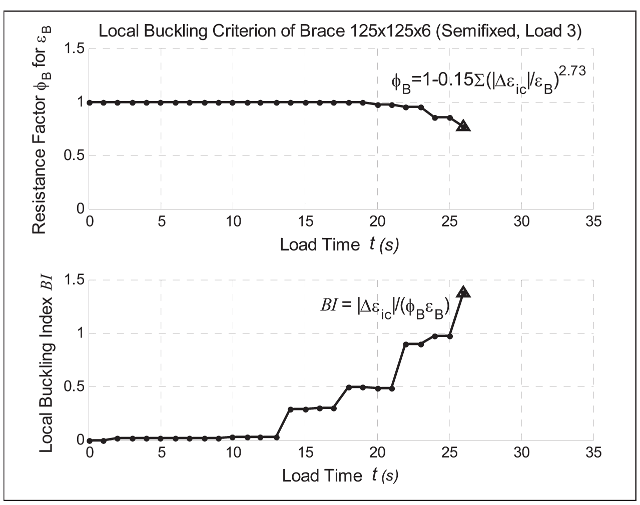

Fig. 22b. Local buckling index of brace 125×125×6 semi-fixed under load 3.

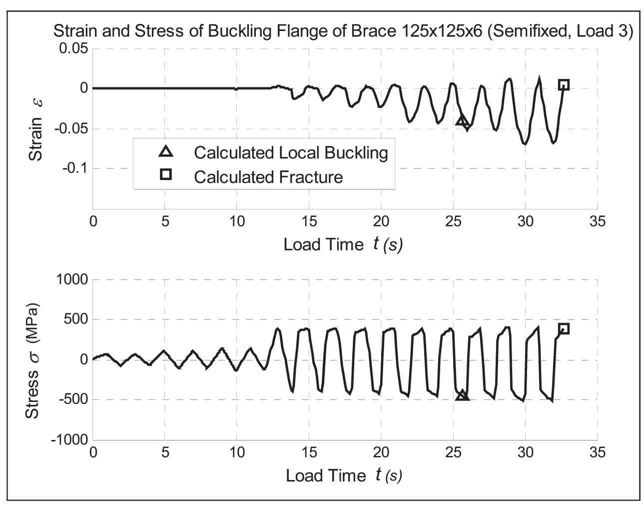

Fig. 22c. Nominal strain and stress of brace 125×125×6 semi-fixed under load 3.

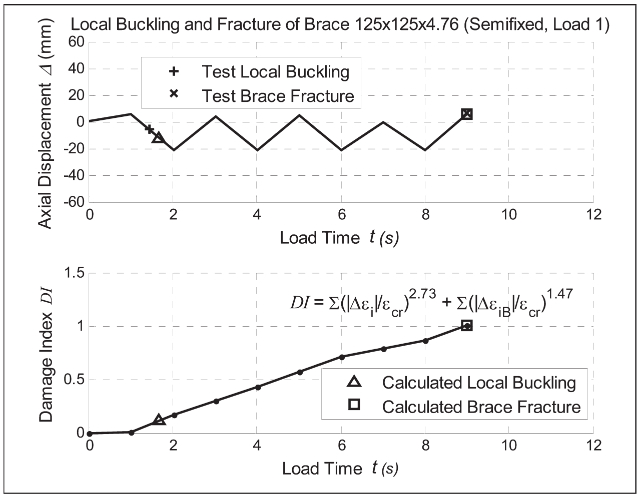

Fig. 23a. Local buckling and fracture of brace 125×125×4.76 semi-fixed under load 1.

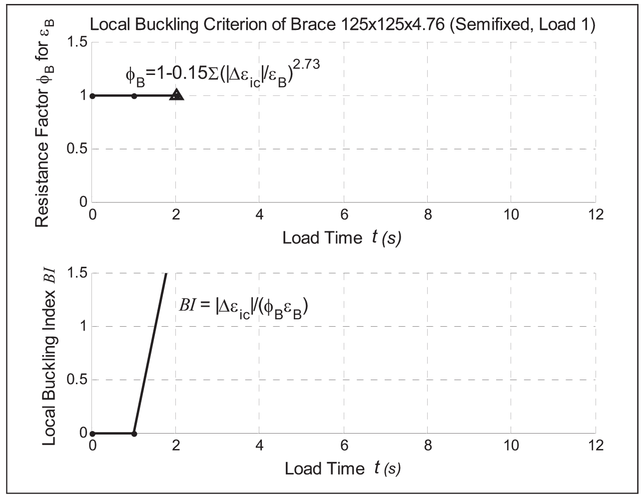

Fig. 23b. Local buckling index of brace 125×125×4.76 semi-fixed under load 1.

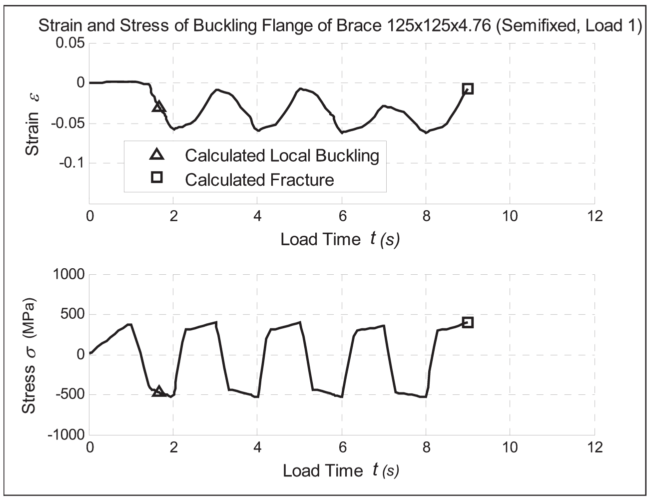

Fig. 23c. Nominal strain and stress of brace 125×125×4.76 semi-fixed under load 1.

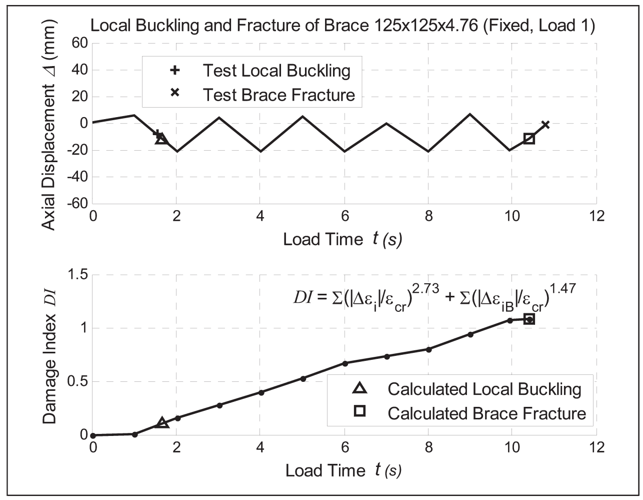

Fig. 24a. Local buckling and fracture of brace 125×125×4.76 fixed under load 1.

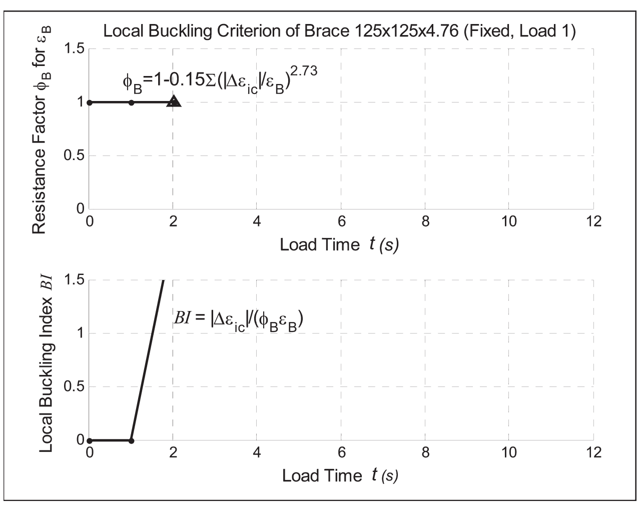

Fig. 24b. Local buckling index of brace 125×125×4.76 fixed under load 1.

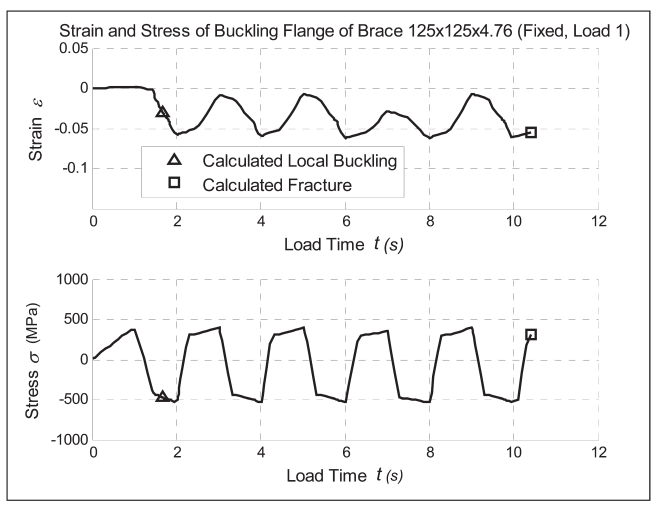

Fig. 24c. Nominal strain and stress of brace 125×125×4.76 fixed under load 1.

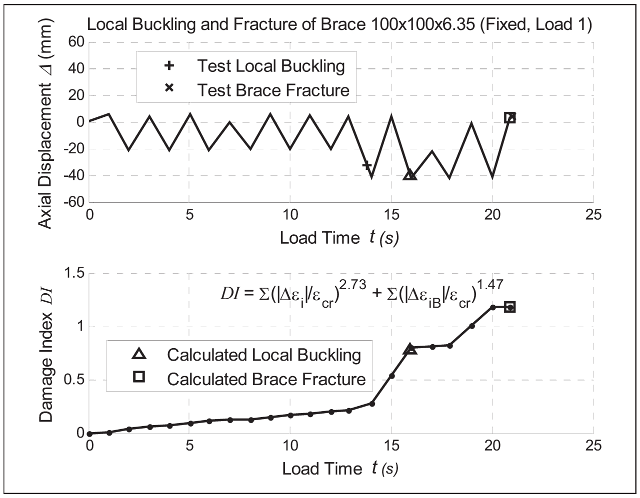

Fig. 25a. Local buckling and fracture of brace 100×100×6.35 fixed under load 1.

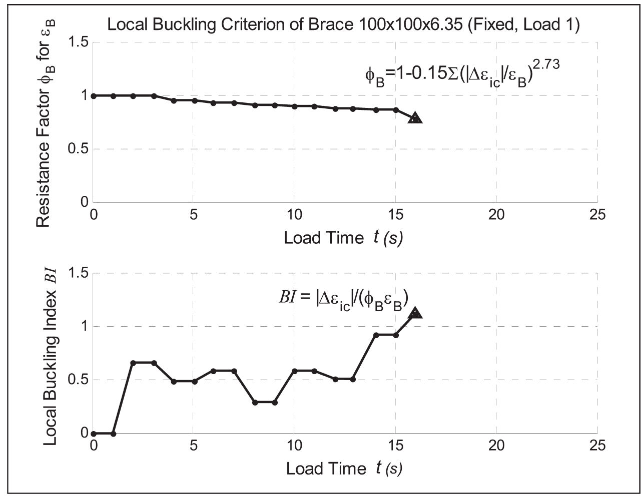

Fig. 25b. Local buckling criterion and index of brace 100×100×6.35 fixed under load 1.

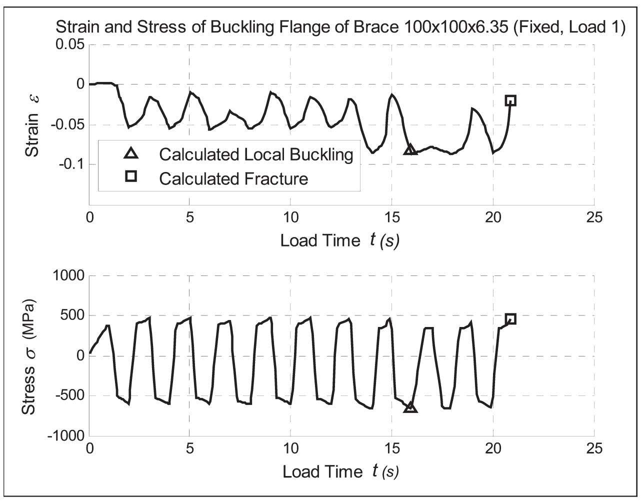

Fig. 25c. Nominal strain and stress of brace 100×100×6.35 semi-fixed under load 1.

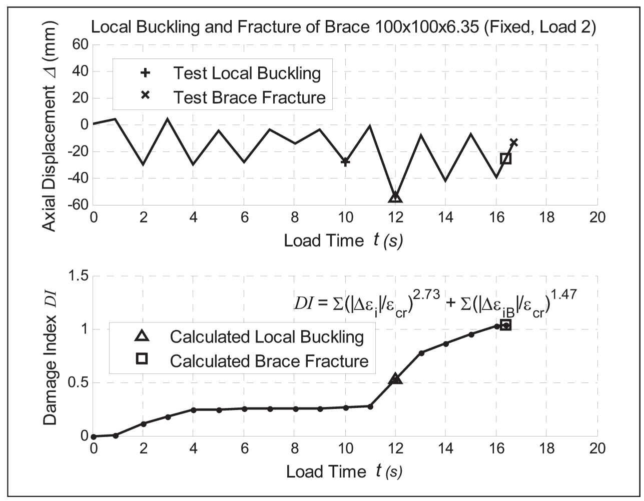

Fig. 26a. Local buckling and fracture of brace 100×100×6.35 fixed under load 2.

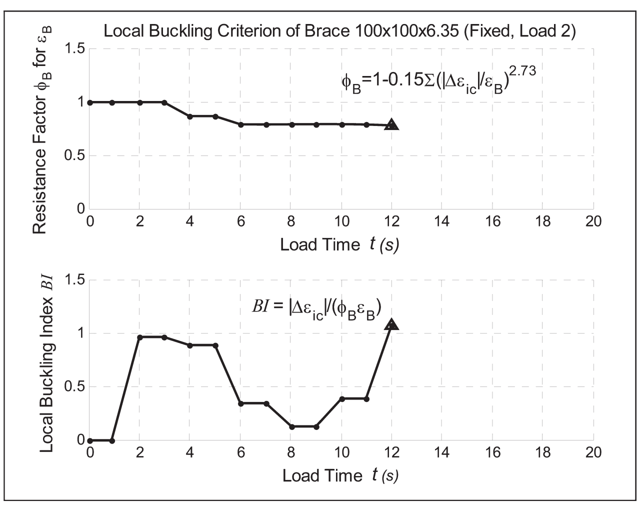

Fig. 26b. Local buckling criterion and index of brace 100×100×6.35 fixed under load 2.

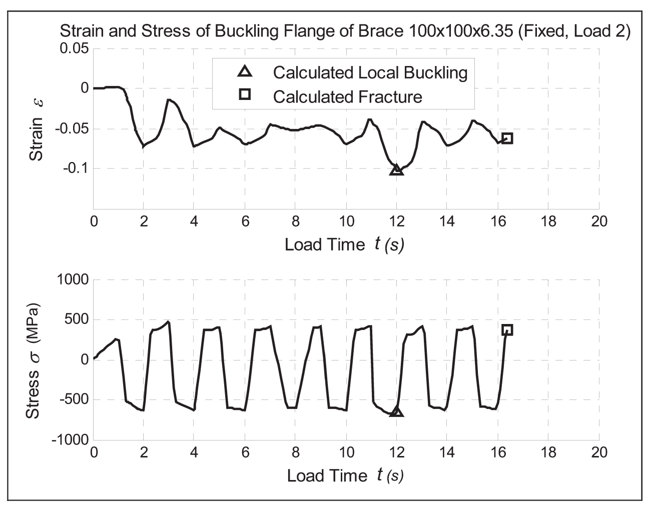

Fig. 26c. Nominal strain and stress of brace 100×100×6.35 fixed under load 2.

CONCLUSIONS

Nominal strain of RHS braces computed through using refined beam elements has been successfully applied to the prediction of local buckling and fracture of RHS braces. The brace tests and partial shell element model simulation also verified the prediction of local buckling by the nominal strain at the flanges. The damage index approach interprets damage accumulation by introducing nominal strain amplitude in a beam element. Comparison of prediction of brace local buckling and fracture using nominal strain and the test results shows good agreement. Thus, brace fracture in structural systems can be investigated efficiently and accurately by using the refined beam element model.

ACKNOWLEDGMENT

This research was supported by grant CMS 02-18703 from the National Science Foundation. This support is gratefully acknowledged.

REFERENCES

Abaqus (2004), "Abaqus Version 6.5 Documentation."

AISC (2005a), *Specification for Structural Steel Buildings*, American Institute of Steel Construction, Chicago, IL.

AISC (2005b), *Seismic Provisions for Structural Steel Buildings*, American Institute of Steel Construction, Chicago, IL.

AISC (2005c), *Steel Construction Manual*, 13th ed., American Institute of Steel Construction, Chicago, IL.

Ding, X. and Foutch, D.A. (2006), "Redundancy in Steel Braced Frames under Seismic Excitations," SRS. No. 640, Department of Civil and Environmental Engineering, University of Illinois at Urbana-Champaign, Urbana, IL, June.

Goel, S.C. and El-Tayem A.A. (1986), "Cyclic Load Behavior of Angle X-Bracing," *Journal of Structural Engineering*, Vol. 112, No. 11, pp. 342–361.

Gu, J.X. and Chan, S.L. (2004), "Second-Order Analysis and Design of Steel Structures Allowing for Member and Frame Imperfections," *International Journal for Numerical Methods in Engineering*, Vol. 62, No. 5, pp. 601–615.

Gugerli, H. and Goel, S.C. (1984), "Inelastic Cyclic Behavior of Steel Bracing Members," Report No. UMEE 82R1, Department of Civil Engineering, University of Michigan, Ann Arbor, MI.

Han, S-W, Wook, T-K and Foutch, D.A. (2006). "Experimental Study of HSS Braces under Cyclic Loads," SRS No. 641, Department of Civil and Environmental Engineering, University of Illinois at Urbana-Champaign, Urbana, IL.

Ikeda, K. and Mahin, S. A. (1986), "Cyclic Response of Steel Braces," *Journal of Structural Engineering*, Vol. 112, No. 5, pp. 342–361.

Jain, A.K., Goel, S.C. and Hanson, R.D. (1978), "Inelastic Response of Restrained Steel Tubes," *Journal of Structural Engineering,* Vol. 104, No. 6, pp. 897–910.

Kahn, L.F. and Hanson, R.D. (1976), "Inelastic Cycles of Axially Loaded Steel Members," *Journal of Structural Engineering*, Vol. 102, No. 5, pp. 947–959.

Lapovok, R., Smirnov, S. and Shveykin, V. (2000), "Damage Mechanics for Fracture Prediction of Metal Forming Tools," *International Journal of Fractures*, Vol. 103, No. 2, pp. 111–126.

Lee, S. and Goel, S.C. (1987), "Seismic Behavior of Hollow and Concrete-Filled Square Tubular Bracing Members," Research Report No. UMCE 87-11, University of Michigan, Ann Arbor, MI.

Liu, Z. (1987), "Investigation of Concrete-Filled Steel Tubes under Cyclic Bending and Buckling," PhD Thesis, University of Michigan, Ann Arbor, MI.

Popov, E.P. and Black, R.G. (1981), "Steel Struts under Cyclic Loadings," *Journal of Structural Engineering*, Vol. 107, No. 9, pp. 1857–1881.

Remennikov, A.M. and Walpole W.R. (1997), "Analytical Prediction of Seismic Behavior for Concentrically-Braced Steel Systems," *Earthquake Engineering and Structural Dynamics*, Vol. 26, No. 8, pp. 859–874.

Venson, A. and Voyiadjis, G. (2001), "Damage Quantification in Metal Matrix Composites," *Journal of Engineering Mechanics*, Vol. 127, No. 3, pp. 291–298.